Journal of Power Sources 196 (2011) 7110–7116

Contents lists available at ScienceDirect

Journal of Power Sources

journal homepage: www.elsevier.com/locate/jpowsour

# Physico-chemical properties of $Ln_{0.5}A_{0.5}Co_{0.5}Fe_{0.5}O_{3-\delta}$ (Ln: La, Sm; A: Sr, Ba) cathode materials and their performance in electrolyte-supported Intermediate Temperature Solid Oxide Fuel Cell

Konrad Świerczek*

*Department of Hydrogen Energy, Faculty of Energy and Fuels, AGH University of Science and Technology, al. Mickiewicza 30, 30-059 Krakow, Poland*

ARTICLE INFO

*Article history:*
Received 16 August 2010
Accepted 23 August 2010
Available online 30 August 2010

*Keywords:*
Perovskite oxide
Crystal structure
Transport properties
Cathode material
SOFC

ABSTRACT

Oxides with perovskite structure and composition: $La_{0.5}Sr_{0.5}Co_{0.5}Fe_{0.5}O_{3-\delta}$, $La_{0.5}Ba_{0.5}Co_{0.5}Fe_{0.5}O_{3-\delta}$, $Sm_{0.5}Sr_{0.5}Co_{0.5}Fe_{0.5}O_{3-\delta}$ and $Sm_{0.5}Ba_{0.5}Co_{0.5}Fe_{0.5}O_{3-\delta}$ were synthesized by a sol–gel EDTA based method. Their physico-chemical properties were evaluated by structural (XRD), transport (electrical conductivity, Seebeck coefficient), and high temperature oxygen nonstoichiometry measurements (TG, $\delta$). A distorted perovskite structure was observed for all of the samples, varying with A-site average radius of cations and tolerance factor *t*. TG measurements, which were performed in air and in reducing atmosphere allowed to determine the initial, as well as the high temperature dependence of the oxygen nonstoichiometry $\delta$ for all materials. At high temperatures the electrical conductivity of the measured samples showed a characteristic maximum and corresponding increase of the Seebeck coefficient. Both effects can be interpreted as a result of a formation of the oxygen vacancies. Apart from $Sm_{0.5}Ba_{0.5}Co_{0.5}Fe_{0.5}O_{3-\delta}$ composition, all other materials possess very high electrical conductivity at high temperatures, well exceeding 100 S cm$^{-1}$. A custom made IT-SOFC cells were constructed with $Ce_{0.85}Gd_{0.15}O_{1.925}$ sinters as a support. Their performance was evaluated in 600–800 °C range. Despite rather similar transport properties of $La_{0.5}Sr_{0.5}Co_{0.5}Fe_{0.5}O_{3-\delta}$, $La_{0.5}Ba_{0.5}Co_{0.5}Fe_{0.5}O_{3-\delta}$ and $Sm_{0.5}Sr_{0.5}Co_{0.5}Fe_{0.5}O_{3-\delta}$ perovskites, the best electrochemical properties were recorded in case of the cell with $La_{0.5}Sr_{0.5}Co_{0.5}Fe_{0.5}O_{3-\delta}$ based cathode.


## 1. Introduction

Designing cathode material for SOFC technology is always a compromise between optimization of its structural, transport, catalytic, thermo-mechanical and other physico-chemical properties as well as its chemical stability towards electrolyte and interconnector. For high temperature (900–1000 °C) cells, LSM ($La_{1-x}Sr_xMnO_3$) based cathode materials and YSZ ($Zr_{1-x}Y_xO_{2-x/2}$) electrolytes perform with sufficient effectiveness. In case of cells working in the intermediate temperature range (600–800 °C) a decrease of the performance may be overcome by an application of composite cathodes or/and usage of new, better materials [1–3]. Nowadays large number of iron-, cobalt-, nickel- or copper-containing oxides are studied in terms of their possible application. Majority of them crystallize in cubic or pseudo-cubic perovskite structure or belong to Ruddlesden–Popper series as well as to other intergrowth-type oxides. Among many others, LSCF ($La_{1-x}Sr_xCo_{1-y}Fe_yO_{3-\delta}$) oxides seem to be particularly interesting [4–6].

A substantial improvement of SOFC performance may be achieved by an implementation of cathode material, which apart from high catalytic activity and appropriate thermo-mechanical properties possess a high mixed ionic-electronic conductivity [7,8]. For such high mixed conductivity a large concentration of mobile oxygen carriers is required. In case of simple $ABO_{3-\delta}$ perovskites the oxygen vacancies act as the ionic charge carriers and the oxygen nonstoichiometry $\delta$ is mainly determined by the amount of +2 cations (Sr, Ba), which substitute +3 cations in A sublattice (La, Sm, Pr). This substitution may be complete and, for instance, in case of $Ba_{0.5}Sr_{0.5}Co_{0.8}Fe_{0.2}O_{3-\delta}$ perovskite very promising properties were observed [9]. However if $\delta$ increases significantly between the room temperature and the working temperature of the cell, a so called chemical expansion of the material will appear, which may significantly increase its thermal expansion coefficient [10].

In this work a series of measurements of a basic physico-chemical properties of isovalence, 50:50 substituted $Ln_{0.5}A_{0.5}Co_{0.5}Fe_{0.5}O_{3-\delta}$ (Ln: La, Sm; A: Sr, Ba) oxide materials were conducted in order to properly characterize the above

* Tel.: +48 12 617 2026; fax: +48 12 617 2522.
*E-mail address:* xi@agh.edu.pl.

0378-7753/$ – see front matter © 2010 Elsevier B.V. All rights reserved.
doi:10.1016/j.jpowsour.2010.08.063

perovskites. A custom made IT-SOFC cells were constructed and their electrochemical characteristics were measured.

## 2. Experimental

Perovskite type oxides with chemical composition $La_{0.5}Sr_{0.5}Co_{0.5}Fe_{0.5}O_{3-\delta}$ (abbreviated in this work as LaSr55), $La_{0.5}Ba_{0.5}Co_{0.5}Fe_{0.5}O_{3-\delta}$ (LaBa55), $Sm_{0.5}Sr_{0.5}Co_{0.5}Fe_{0.5}O_{3-\delta}$ (SmSr55) and $Sm_{0.5}Ba_{0.5}Co_{0.5}Fe_{0.5}O_{3-\delta}$ (SmBa55) were synthesized using EDTA based, sol–gel method. Details of the procedure can be found elsewhere [11]. The final sintering of the materials was performed at 1200 °C in air with slow cooling to the room temperature (RT). Structural studies at RT were performed using Phillips X'Pert Pro diffractometer in 10–90° range with $CuK_\alpha$ radiation. The X-ray patterns were analyzed using Rietveld method with GSAS/EXPGUI set of software [12,13]. For LaSr55 sample additional high temperature XRD studies were conducted at 400, 600 and 800 °C. In order to make a comparison between the obtained structural results, unit cell volume and unit cell parameters were appropriately normalized to a pseudo-cubic perovskite cell. Goldschmidt's tolerance factor $t=(r_A+r_B)/(2^{0.5}(r_B+r_O))$ ($r_i$ – appropriate ionic radii), which describes distortion of the perovskite structure was calculated using two different methods: $t_{BV}$ was calculated using SPUDS software [14], which uses Bond Valence method [15], $t_g$ defined in [16] was calculated using geometric average of the interatomic distances obtained from the structural studies. It is necessary to mention that in case of XRD measurements, oxygen positions in the unit cell cannot be refined with high precision and the obtained $t_g$ values may contain significant error. Thermogravimetric measurements (TG) were performed on TA Instruments Q5000 IR apparatus in RT–1000 °C range. Relatively slow heating rates were used: 1° min$^{-1}$ in case of measurements performed in air and 0.5° min$^{-1}$ for reduction measurements, which were conducted in 0.1% $H_2$ in Ar atmosphere. Before the actual measurements, for all the samples initial heating and cooling runs were performed with 1° min$^{-1}$ rate in RT–1000 °C range. These initial runs, together with the reduction runs (see below), allowed for an estimation of the oxygen nonstoichiometry present in the "as prepared" samples, indicated as $\delta$ in Table 1. The difference between these values and the equilibrium ones can be interpreted as due to an insufficiently slow rate of cooling from 1200 °C to RT. Samples reduced on TG were characterized in terms of their crystal structure by XRD technique. Transport properties of the materials were characterized by a high temperature electrical conductivity, measured using a four-probe DC method and Seebeck coefficient measurements, which were performed by means of a dynamic method with temperature gradient equal 2–3 °C. Due to an influence of oxygen stoichiometry, as well as because of moisture sensitivity of the samples, both measurements were performed during cooling with 1° min$^{-1}$ rate. Two-electrode electrolyte-supported SOFC cells were constructed using relatively thick (600-800 μm) $Ce_{0.85}Gd_{0.15}O_{1.925}$ sinters having >95% theoretical density. Sintering of the electrolyte pellets was conducted at 1500 °C. A rather typical, 40 wt.% 8YSZ/60 wt.% NiO cermet was used as the anode material. Anode firings were done at 1200 °C, with additional step at 400 °C, at which organic binder of the anode paste decomposes. Cathode paste was prepared by mixing of the cathode powder with appropriate amount of organic binder, in order to obtain required consistency. Cathode firings were performed at 1100 °C with additional step at 400 °C. For all the cells the area of both electrodes was about 0.25 cm$^2$. IT-SOFC cell performance was studied using home-made SOFC testing unit equipped with Solartron SI 1287 electrochemical interface and Solartron 1252A frequency response analyzer. Dry hydrogen flow of 100 cm$^3$ min$^{-1}$ was applied on the anode side, while air was provided at the cathode side with flow rate of about 500 cm$^3$ min$^{-1}$. The impedance spectra and the current density–voltage characteristics were measured in 600–800 °C range. The impedance spectroscopy measurements were performed under open-circuit conditions in 0.1–300 kHz range with 25 mV amplitude. The interpretation of the results was conducted in accordance with the method presented in Ref. [17]: the ohmic resistance $R_{ohm}$ and the total interfacial polarization resistance (anode | electrolyte $R_a$ plus cathode | electrolyte $R_c$) were evaluated by fitting the impedance spectra to an equivalent circuit consisting of $L$–$R_{ohm}$–$(RQ)_{HF}$–$(RQ)_{LF}$, where $L$ is an inductance, $R$ is the resistance, $Q$ is the constant phase element, while HF and LF stand for correspondingly high-frequency and low-frequency contribution.

## 3. Results and discussion

Structural parameters of the obtained materials are gathered in Table 1. For LaSr55 perovskite a relatively low symmetry, monoclinic $I12/c1$ space group was chosen, on the basis of previous reports, which indicated such a symmetry from neutron studies [18]. Similarly as reported in [18], structural refinement in a more typical $R$-3$c$ group resulted in only little worse refinement statistic. For LaBa55 sample the obtained XRD results could be indexed using cubic symmetry, but choice of tetragonal $I4/mcm$ group gave significantly better refinement statistics, which strongly support existence of tetragonal distortion of the unit cell. In case of SmSr55 material, a relatively low quality data was collected, with a much lower signal/noise ratio, indicating poor crystallinity of the sample. Refinement of the crystal structure in orthorhombic $Pbnm$ space group gave acceptable results, however, data quality makes this conclusion uncertain. For SmBa55 composition, tetragonal, A-site double-perovskite structure was observed, which could be very well indexed with $P4/mmm$ space group. An ordering present in Sm–Ba sublattice is due to a major difference between the ionic radii of the elements ($Sm^{3+}$: 1.24 Å, $Ba^{2+}$: 1.61 Å [19]) and is a known feature of such compounds [20]. As could be seen in Fig. 1, a more or less linear dependence of a normalized unit cell volume as a function of average A-site cation radius was observed. For such iso-

**Table 1**
Structural parameters of LaSr55, LaBa55, SmSr55 and SmBa55 perovskites. The initial oxygen nonstoichiometry $\delta'$ present in "as prepared" samples was evaluated from 1st cycle of TG measurements.

| Composition | LaSr55 | LaBa55 | SmSr55 | SmBa55 |
|---|---|---|---|---|
| Space group | $I12/c1$ | $I4/mcm$ | $Pbnm$ | $P4/mmm$ |
| $a$ [Å] | 5.4419(1) | 5.5320(1) | 5.4039(3) | 3.9107(1) |
| $b$ [Å] | 5.4547(1) | | 5.4270(4) | |
| $\beta$ [°] | 90.216(2) | | | |
| $c$ [Å] | 7.7108(2) | 7.8177(1) | 7.6536(5) | 7.6597(2) |
| Normalized $V$ [Å$^3$] | 57.222(2) | 59.812(1) | 56.114(6) | 58.573(5) |
| $\delta'$ [mol mol$^{-1}$] | 0.01 | 0.02 | 0.04 | 0.19 |
| $\chi^2$; $R_{wp}$ [%]; $R_p$[%] | 0.786; 13.2; 10.3 | 0.758; 14.8; 11.4 | 0.775; 12.4; 9.7 | 0.777; 12.9; 10.0 |

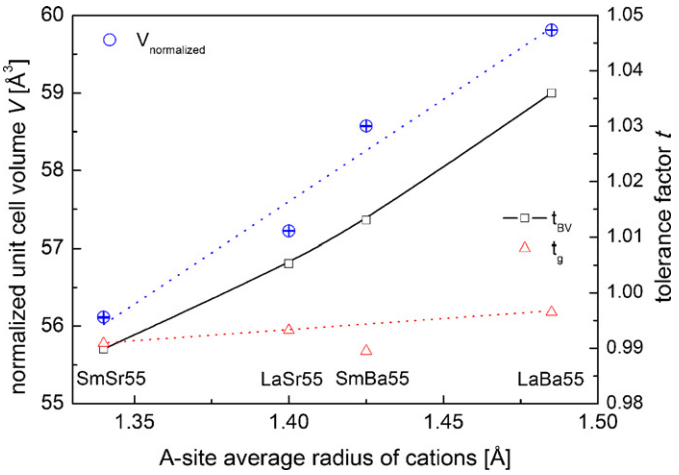


**Fig. 1.** Normalized unit cell volume calculated from XRD measurements together with tolerance factors $t_{BV}$ and $t_g$ as a function of A-site average radius of cations.

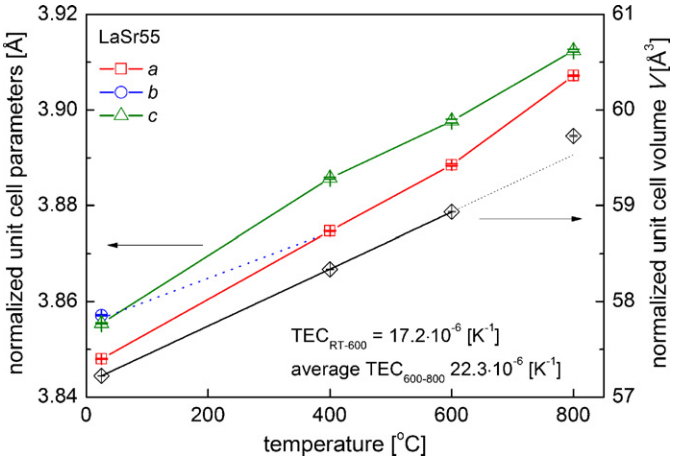


**Fig. 3.** High temperature dependence of normalized unit cell parameters and unit cell volume of LaSr55 perovskite calculated from XRD measurements.

valenece substitution, the deviation from a straight line indicates existence of some additional effects. In case of SmBa55, a visibly higher than expected unit cell volume may be associated with a relatively high oxygen nonstoichiometry of the sample present at RT (Table 1). This effect, as well as the high temperature oxygen nonstoichiometry of the samples is discussed below. Calculated $t_{BV}$ values (Fig. 1) show monotonic dependence on A-site average radius of cations. In case of $t_g$ a significantly lower, less than 1 values were obtained. Lower than expected $t_g$ value for SmBa55 sample may be related to its double-perovskite structure and high values of $\delta$. Apart from it, an expected increase of tolerance factor with the increasing A-site average radius of cations was observed.

Fig. 2 shows microstructure of LaSr55 powder indicating few-micrometer grain size. Similar microstructure was observed for other materials. Despite poor crystallinity of SmSr55 sample, SEM microphotographs revealed almost identical microstructure also in this case, which suggests atomic-scale disorder present in the sample.

In Fig. 3, an evolution of normalized cell parameters of LaSr55 as a function of temperature are presented. The high temperature XRD data strongly suggests existence of *I*4/*mcm* structure of the sample for $T \geq 400\,^{\circ}C$. This in turn indicates a presence of a phase transition from the RT monoclinic *I*12/*c*1 phase (octahedra tilt type $a^-b^-b^-$, according to Glazer [21]) to the high temperature *I*4/*mcm* phase ($a^0a^0c^-$). Due to the nature of the change of the octahedra tilt, such phase transition must be of the first order type [20,22]. Further, precise neutron studies are required to unambiguously describe the observed structural changes. Nevertheless, the observed unit cell volume dependence on temperature is rather linear up to 600 °C. It allows for a calculation of thermal expansion coefficient, TEC, which equals $17.2 \times 10^{-6}\,K^{-1}$ in RT–600 °C range. At higher temperatures TEC increases, which indicates influence of chemical expansion [23]. As the oxygen nonstoichiometry increases, the additional two electrons left in the crystal by escaping oxygen are trapped on higher valence cations and increase their radii. It is manifested by a stronger unit cell volume dependence on temperature and consequently higher TEC values [10]. This effect is responsible for higher than expected unit cell volume of SmBa55 sample (Table 1), due to a significantly high oxygen nonstoichiometry present in the sample at RT.

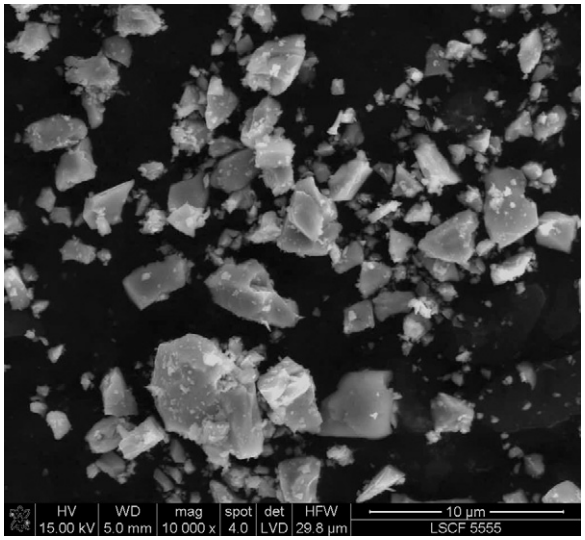


**Fig. 2.** SEM microphotograph of LaSr55 indicating few-micrometer size of the obtained powder.

In Fig. 4, thermogravimetric data (taken on the second run) of a controlled reduction of LaSr55 perovskite in 0.1 $H_2$ in Ar atmosphere are presented. At around 700 °C a clearly visible plateau is present. In the temperature range above 900 °C another plateau appears. XRD studies performed on the reduced at 1000 °C material indicate a decomposition of the sample into mixture of tetragonal *I*4/*mmm* $LaSrFeO_4$ and metallic Co. In Fig. 5, structural data together with Rietveld refinement of such mixture are presented.

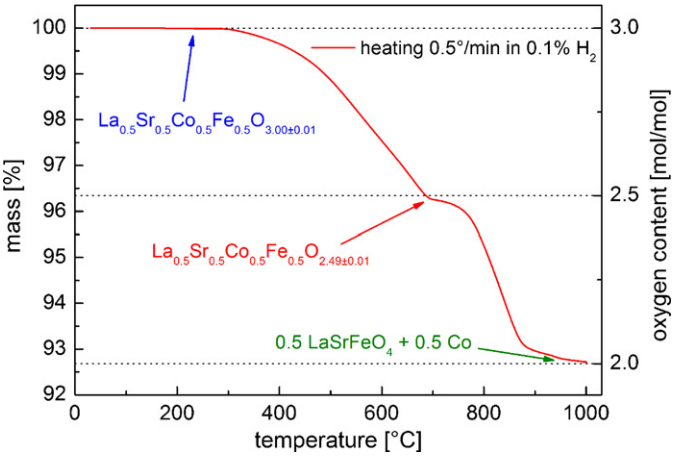


**Fig. 4.** Changes of LaSr55 mass observed on TG during controlled reduction in 0.1% $H_2$ in Ar atmosphere.

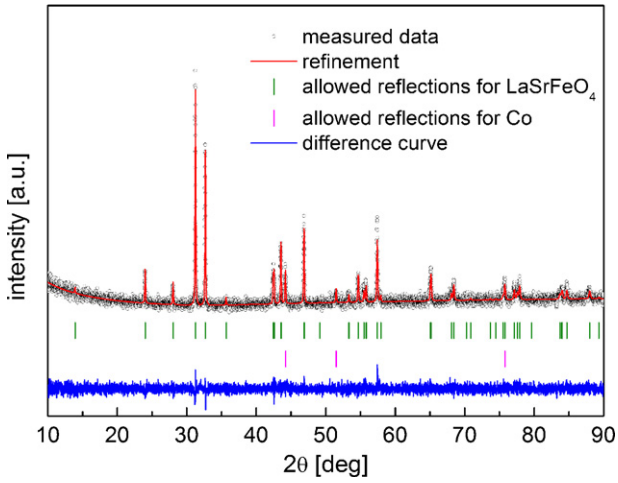


**Fig. 5.** XRD diffraction pattern of the reduced at 1000 °C LaSr55 sample.

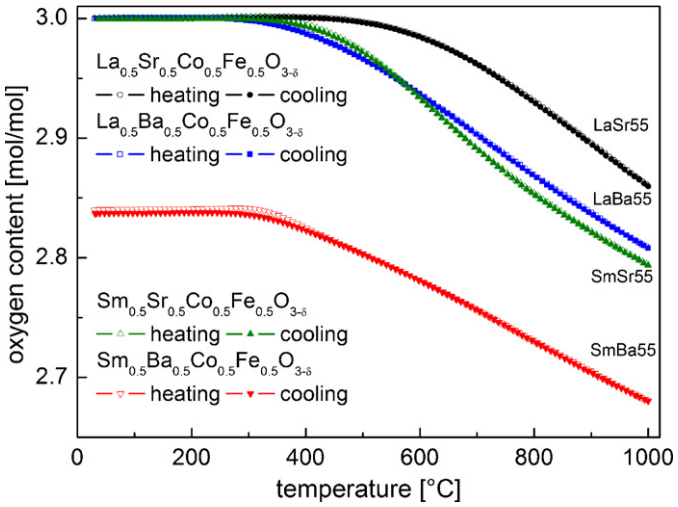


**Fig. 6.** Temperature dependence of the oxygen nonstoichiometry $\delta$ in air for the obtained perovskite oxides. Data calculated from TG measurements in air.

Weight percentage of $LaSrFeO_4$ phase in the mixture was refined to be 88(3)%, which is in a relatively good agreement with a theoretical value of 83% for such decomposition. Therefore a two-step reduction mechanism of LaSr55 may be presented as follows:

$$La_{0.5}Sr_{0.5}Co_{0.5}Fe_{0.5}O_3 \rightarrow La_{0.5}Sr_{0.5}Co_{0.5}Fe_{0.5}O_{3-\delta} + \delta/2O_2\uparrow, \quad 0 \leq \delta \leq 0.5 \tag{1}$$

$$La_{0.5}Sr_{0.5}Co_{0.5}Fe_{0.5}O_{2.5} \rightarrow (1/2)LaSrFeO_4 + (1/2)Co + (1/4)O_2\uparrow \tag{2}$$

Calculation of the initial as well as the temperature dependence of $\delta$ for LaSr55 can be done using the above equations. According to reaction (2), the final oxygen content in the sample equals to 2 moles per mole. Assuming that the observed mass loss of the sample equal 7.3% at 1000 °C in relation to RT (Fig. 4) is only due to the oxygen, one may calculate the initial oxygen content present in LaSr55. The obtained value equals $3.00 \pm 0.01$ mol mol$^{-1}$ ($\delta = 0.00 \pm 0.01$ mol mol$^{-1}$), which agrees with previous measurements [18]. Moreover, a quite good agreement of the brownmillerite composition $La_{0.5}Sr_{0.5}Co_{0.5}Fe_{0.5}O_{2.49\pm0.01}$ can be observed. It must be pointed out that $LaSrFeO_4$ phase may as well possess deviation from the oxygen stoichiometry, but the calculated unit cell parameters for this phase indicate rather stoichiometric composition. While the existence of $Fe^{3+}$ containing $LaSrFeO_4$ phase after reduction is somewhat surprising, it is clearly proven by the XRD results and by lack of any changes of mass on cooling from 1000 °C. Additionally, an attempt to structurally characterize $La_{0.5}Sr_{0.5}Co_{0.5}Fe_{0.5}O_{2.49\pm0.01}$ material was made, however it partially oxidized in air at room temperature. The obtained XRD data revealed existence of two-phase mixture containing $ABO_{2.5}$ brownmillerite and $ABO_{3-\delta}$ pseudo-cubic perovskite phases.

Analogous to the described above behaviour was observed for SmSr55 sample and it allowed for a similar calculation of the oxygen nonstoichiometry. However reduction of LaBa55 and SmBa55 materials differed considerably. In these cases, multiphase systems with some unidentified phases were observed after reduction at 1000 °C, suggesting different mechanism of reduction, comparing to reaction (2). Nevertheless, the first plateau, indicating presence of the brownmillerite type phase was present also in these samples. This plateau, which was ascribed to stoichiometric $ABO_{2.5}$ composition, allowed for an estimation of the initial oxygen content in LaBa55 ($\delta = 0.00$ mol mol$^{-1}$) and SmBa55 ($\delta = 0.16$ mol mol$^{-1}$). The presented results can be summarized that apart from SmBa55 all other samples have stoichiometric composition while very slowly cooled to RT.

The initial values of $\delta$ together with slow TG runs performed in air allowed for the calculation of temperature dependence of absolute values of the oxygen nonstoichiometry. Data for all of the obtained materials are gathered in Fig. 6. As can be seen, fair overlap of the heating and cooling runs strongly indicates that the obtained values represent the high temperature equilibrium $\delta$ present in the samples. In case of LaSr55, a significant deviation from the stoichiometry appears above 500 °C. For LaBa55 and SmSr55 $\delta$ increases above around 400 °C. SmBa55 possesses high oxygen nonstoichiometry at RT, it further increases at temperatures above 300 °C. This high nonstoichiometry is directly related to the crystal structure, as the oxygen position 1*d* (1/2, 1/2, 1/2) in the unit cell, which is located in the plane of smaller cations ($Sm^{3+}$) is unfavourable in such double-perovskite [24]. Additionally, oxygen content refinement from XRD data suggests similar, high $\delta$ for SmBa55 sample, but due to a low sensitivity of XRD measurements for oxygen, this result can only be a supplementary one to the TG results. Data presented in Fig. 6 allows to estimate an enthalpy of formation of the oxygen vacancies for the measured

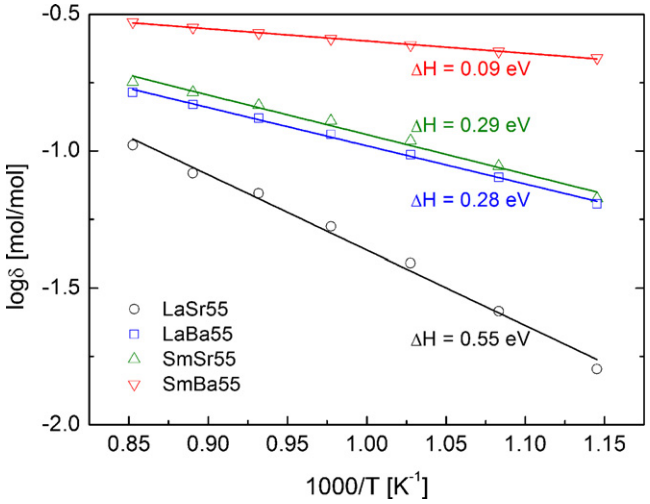


**Fig. 7.** Arrhenius-type plot for the calculation of the enthalpy of formation of the oxygen vacancies at high temperatures. Equilibrium values of $\delta$ taken from TG measurements in air.

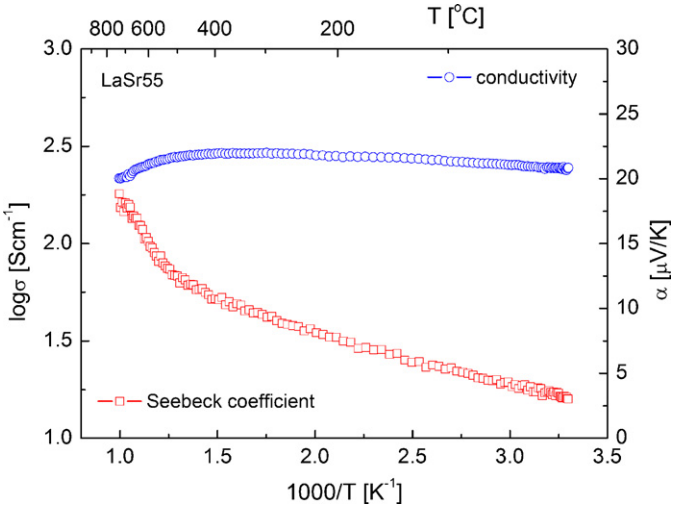


**Fig. 8.** High temperature electrical conductivity and Seebeck coefficient of LaSr55 perovskite.

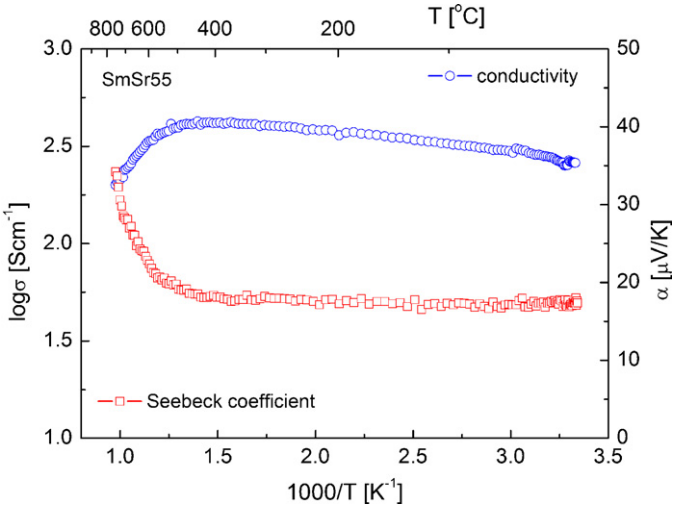


**Fig. 10.** High temperature electrical conductivity and Seebeck coefficient of SmSr55 perovskite.

perovskites (Fig. 7). It is worth noting an especially low value of $\Delta H$ equal 0.09 eV for SmBa55 composition. It may be correlated with the above mentioned 1*d* oxygen position, which tends to be highly unoccupied. Further, possibly neutron structural studies are needed in order to determine temperature-induced changes of occupancy for all oxygen sites in this material. Summarizing oxygen nonstoichiometry results, one may notice significant $\delta$ in the 600–800 °C range present for all samples, which should be beneficial in terms of the application of these materials in IT-SOFC cells. The high temperature oxygen nonstoichiometry increases in the following way: LaSr55 < LaBa55 < SmSr55 < SmBa55. It is worth noting that it does not follow the unit cell volume dependence (Fig. 1).

In Figs. 8–11, the high temperature transport properties of the obtained materials are presented. Total electrical conductivity and Seebeck coefficient data are presented together, in Arrhenius-type plot. As can be noticed, apart from SmBa55 sample, all other materials possess very high electrical conductivity, well above required 100 S cm$^{-1}$ for the cathode materials. A corresponding, low, positive values of Seebeck coefficient were recorded. A characteristic maxima can be seen on $\sigma$ curves. They correspond well with the TG curves and therefore can be interpreted as a result of a formation of the oxygen vacancies:

$$O_O \rightarrow V_O^{\bullet\bullet} + 2e^- + 0.5O_2\uparrow \quad (3)$$

Electrons created in the above process are trapped on the higher valence 3*d* metals and, as a result, lower their average valence. This in turn decreases $[Me^{n+}][Me^{(n+1)+}]$ product, and therefore lowers the effective carrier concentration of the hopping mechanism [7]. Additional hindrance of the transport properties is due to a break of Me–O–Me double exchange in case of the oxygen vacancy presence. The ionic component of the electrical conductivity is too low to have significant impact on the observed total values [4,25]. A corresponding increase of Seebeck coefficient, visible at higher temperatures, can be interpreted as due to an increase of the positive component of $\alpha$ (hole transport). Additionally, ionic Seebeck of mobile oxygen vacancies will add up to the observed values, however, the magnitude of this effect is unknown. Unfortunately, due to the existence of mixed valence, possibly for both Co and Fe cations, as well as because of the possible reaction of charge disproportionation in case of Fe, more detailed description of the transport properties would require knowledge of the charge and spin state of 3*d* metals and is beyond scope of this research. In

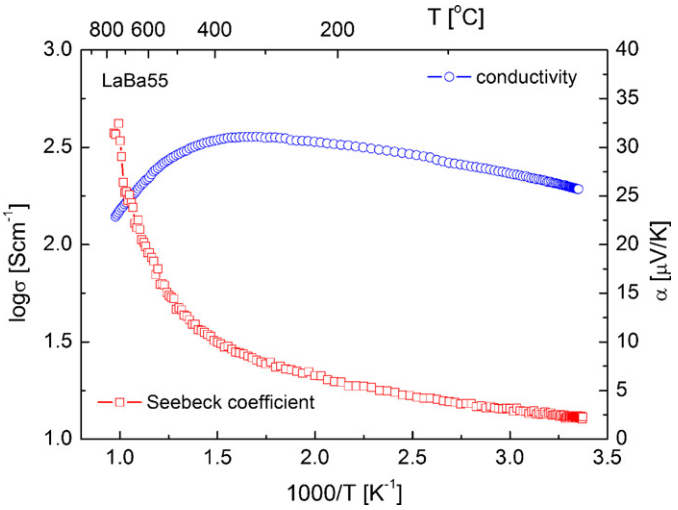


**Fig. 9.** High temperature electrical conductivity and Seebeck coefficient of LaBa55 perovskite.

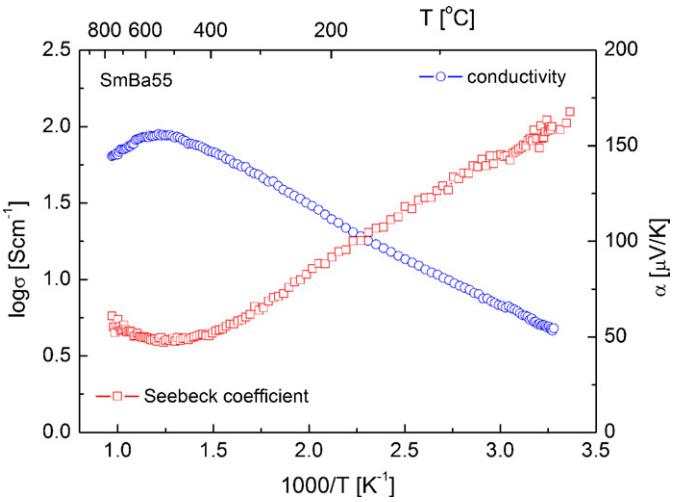


**Fig. 11.** High temperature electrical conductivity and Seebeck coefficient of SmBa55 perovskite.

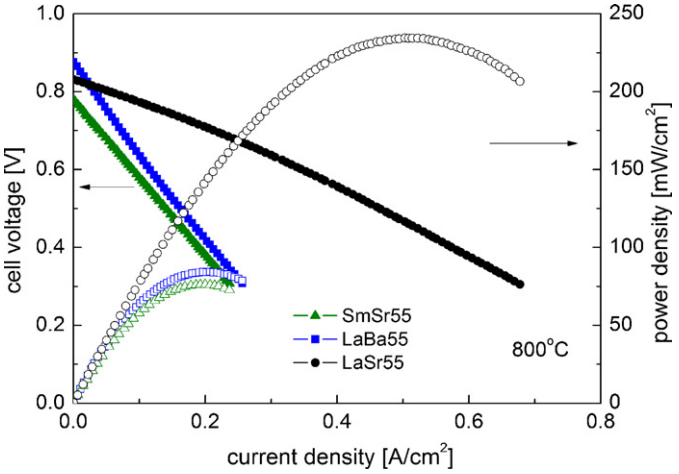


**Fig. 12.** Current density–voltage and corresponding power density characteristics of IT-SOFC cells with LaSr55, LaBa55 and SmSr55 based cathodes. Measurements were performed at 800 °C.

case of SmBa55 a significantly lower electrical conductivity and a much higher, positive values of Seebeck coefficient were observed (Fig. 11). This result can be expected taking into account high value of $\delta$, which decreases the average 3*d* metal valence down to +3.18 at RT. For other samples, the initial average valence should be close to +3.5, assuming lack of the oxygen nonstoichiometry.

The presented above characterization of basic physico-chemical properties of $Ln_{0.5}A_{0.5}Co_{0.5}Fe_{0.5}O_{3-\delta}$ (Ln: La, Sm; A: Sr, Ba) oxides, which indicated high values of $\delta$ and high total electrical conductivity, suggests that all of them can be possibly used as cathode materials in IT-SOFC cells. LaSr55, LaBa55 and SmSr55 based cathode pastes were successfully applied and sintered on $Ce_{0.85}Gd_{0.15}O_{1.925}$ pellets. In case of SmBa55 perovskite, possibly due to an incompatibility of the thermo-mechanical properties, it was not possible to obtain sintered cathode layer with good adhesion to the electrolyte. In Fig. 12, a typical current density–voltage and corresponding power density characteristics of IT-SOFCs with LaSr55, LaBa55 and SmSr55 cathodes are presented. The measurements were performed at 800 °C. Despite identical construction, one may observe significantly higher values of power density, reaching about 230 mW cm$^{-2}$, for the cell containing LaSr55 based cathode in relation to cells with LaBa55 or SmSr55 based cathodes.

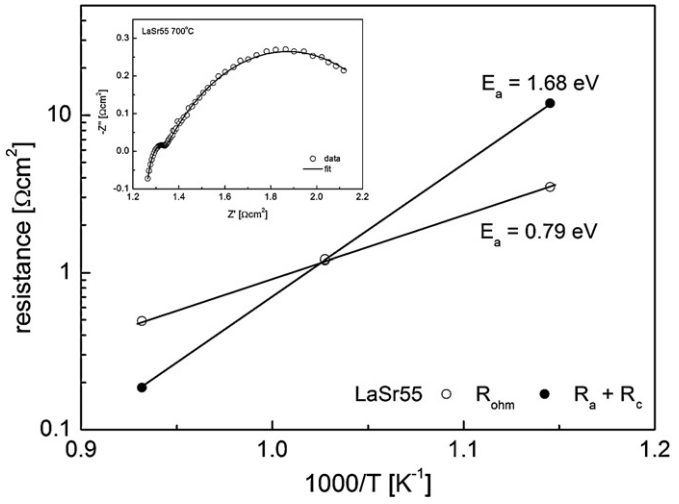


**Fig. 13.** Temperature dependence of calculated values of $R_{ohm}$ and $R_a + R_c$, based on model presented in Ref. [17]. The inlet figure shows typical results of impedance measurements together with the refinement.

Fig. 13 shows refined values of the temperature dependence of $R_{ohm}$ (ohmic resistance) and $R_a + R_c$ (total interfacial polarization resistance) measured for LaSr55 based cell. The inlet in Fig. 13 shows a typical impedance spectrum measured at 700 °C. Calculated activation energy of $R_{ohm}$ equals 0.79 eV and is in excellent agreement with ionic conductivity data for $Ce_{0.85}Gd_{0.15}O_{1.925}$ electrolyte [26]. In case of LaBa55 and SmSr55 based cells the calculated values of ohmic resistance and total interfacial polarization resistance were significantly higher: $R_{ohm} = 1.70\ \Omega\ cm^2$ and $R_a + R_c = 1.80\ \Omega\ cm^2$ at 800 °C for LaBa55 cell; $R_{ohm} = 2.85\ \Omega\ cm^2$ and $R_a + R_c = 2.03\ \Omega\ cm^2$ at 800 °C for SmSr55 cell. Apart from the cathode used, construction of all of the cells was identical. Because of that and due to the fact that all of the cathode materials exhibit similar total electrical conductivity one may assume that the observed high values of $R_{ohm}$ show increased resistance on the between electrolyte and cathode layer. This suggest thermo-mechanical incompatibility, particularly presence of chemical expansion for highly oxygen deficient samples, which can significantly affect resistance between cathode layer and electrolyte. This would also explain high values of total interfacial polarization resistance measured for these cells. Further studies are needed to clarify these results. Nevertheless, the obtained results for LaSr55 suggest very good catalytic activity of this perovskite, in relation to the oxygen reduction reaction, which takes place at the cathode. While the performance of the constructed LaSr55 based cell was rather not impressive, much higher power outputs, especially above 700 °C (Fig. 13), could be expected for cells having thinner electrolyte.

## 4. Conclusions

The performed characteristics of the physico-chemical properties of $Ln_{0.5}A_{0.5}Co_{0.5}Fe_{0.5}O_{3-\delta}$ (Ln: La, Sm; A: Sr, Ba) materials revealed distorted perovskite structure and high values of the high temperature electrical conductivity in case of LaSr55, LaBa55 and SmSr55 oxides. The oxygen nonstoichiometry $\delta$ at high temperatures increases in the following way: LaSr55 < LaBa55 < SmSr55 < SmBa55. The characteristic maxima observed on the electrical conductivity dependence and corresponding increase of Seebeck coefficient at high temperatures are correlated to the increase of the oxygen nonstoichiometry. Constructed IT-SOFC cells with LaBa55 and SmSr55 based cathodes exhibited high values of ohmic resistance and total interfacial polarization resistance, possibly due to the thermo-mechanical incompatibility. In case of LaSr55 based cell, relatively good performance was measured, suggesting high catalytic activity of this cathode material.

## Acknowledgement

Author would like to thank Mr. Takeshi Saito for fruitful discussions. This work was supported by Polish Ministry of Science and Higher Education under grant No. N507 3545 35.

## References

[1] J.W. Fergus, R. Hui, X. Li, D.P. Wilkinson, J. Zhang, (Eds.), Solid Oxide Fuel Cells Materials Properties and Performance, CRC Press, 2009.
[2] S.C. Singhal, K. Kendall, (Eds.), High Temperature Solid Oxide Fuel Cells: Fundamentals, Design and Applications, Elsevier, 2003.
[3] T. Ishihara, (Ed.), Perovskite Oxide for Solid Oxide Fuel Cells, Springer 2009.
[4] E.V. Tsipis, V.V. Kharton, J. Solid State Electrochem. 12 (2008) 1039–1060.
[5] E.V. Tsipis, V.V. Kharton, J. Solid State Electrochem. 12 (2008) 1367–1391.
[6] J. Richter, P. Holtappels, T. Graule, T. Nakamura, L.J. Gauckler, Monatsh Chem. 140 (2009) 985–999.
[7] J. Molenda, K. Świerczek, W. Zając, J. Power Sources 173 (2007) 657–670.
[8] E. Ivers-Tiffée, A. Weber, D. Herbstritt, J. Eur. Ceram. Soc. 21 (2001) 1805–1811.
[9] W. Zhou, R. Ran, Z. Shao, J. Power Sources 192 (2009) 231–246.
[10] K. Świerczek, Solid State Ionics 179 (2008) 126–130.

[11] K. Świerczek, M. Gozu, J. Power Sources 173 (2007) 695–699.
[12] A.C. Larson, R.B. Von Dreele, Los Alamos Natl. Lab. Rep. – LAUR 86-748 (2004).
[13] B.H. Toby, J. Appl. Cryst. 34 (2001) 210–213.
[14] M.W. Lufaso, P.M. Woodward, Acta Cryst. B57 (2001) 725–738.
[15] I.D. Brown, Phys. Chem. Minerals 15 (1987) 30–34.
[16] B. Dabrowski, O. Chmaissem, J. Mais, S. Kolesnik, J.D. Jorgensen, S. Short, J. Solid State Chem. 170 (2003) 154–164.
[17] Q.L. Liu, K.A. Khor, S.H. Chan, J. Power Sources 161 (2006) 123–128.
[18] K. Świerczek, B. Dabrowski, L. Suescun, S. Kolesnik, J. Solid State Chem. 182 (2009) 280–288.
[19] R.D. Shannon, Acta Cryst A32 (1976) 751–767.
[20] R.H. Mitchell, Perovskites Modern and Ancient, Almaz Press Inc., Canada, 2002.
[21] A.M. Glazer, Acta Cryst. B28 (1972) 3384–3392.
[22] C.J. Howard, H.T. Stokes, Acta Cryst. B54 (1998) 782–789.
[23] M. Ram, Y. Tsur, J. Electroceram. 22 (2009) 120–124.
[24] P. Karen, P.M. Woodward, J. Mater. Chem. 9 (1999) 789–797.
[25] Y. Teraoka, H.M. Zhang, K. Okamoto, N. Yamazoe, Mat. Res. Bull. 23 (1988) 51–58.
[26] W. Zając, J. Molenda, Solid State Ionics 179 (2008) 154–158.